Hindawi
Advances in Materials Science and Engineering
Volume 2022, Article ID 3502383, 15 pages
https://doi.org/10.1155/2022/3502383

Research Article

Electric Discharge Machining of AZ91 Magnesium Hybrid Composites under Different Dielectric Mediums

T. Prakash,[1] **R. Ranjith**,[1] **S. Krishna Mohan**,[2] **and S. Venkatesan**[3]

[1]*Department of Mechanical Engineering, SNS College of Technology, Coimbatore, Tamil Nadu, India*
[2]*Department of Mechanical Engineering, E.G.S. Pillay Engineering College, Nagapattinam, Tamil Nadu, India*
[3]*School of Mechanical Engineering, College of Engineering and Technology, Wachemo University, Hosaena, Ethiopia*

Correspondence should be addressed to S. Venkatesan; profsvenkatesan@gmail.com

Received 14 July 2022; Accepted 6 October 2022; Published 14 October 2022

Academic Editor: Md Mainul Islam

In this work, an attempt was made to machine the AZ91/5B_4C/5Gr hybrid composites in a castor oil electric discharge medium with an objective of attaining green environment. The hybrid composites were produced using stir casting technique in a protective environment. Experiments were conducted by varying dielectric fluid (castor oil and hydrocarbon oil), tool materials (copper, graphite, and brass), polarity, current, pulse-on time, and gap distance in Al_2O_3 mixed dielectric medium. L36 Taguchi approach was adopted for the design of experiments, and machining performance was accessed in terms of material removal rate (MRR), tool wear rate (TWR), and surface roughness (R_a). Because of castor oil's high thermal conductivity, high kinematic viscosity, and lower dielectric strength, the specimen exhibits 5% higher MRR than EDM oil. When the electrodes were connected to the negative polarity, the Ra was 1.72 μm and 3.66 μm at positive polarity; however, at negative polarity, the TWR was higher than the MRR. The high density and specific heat of castor oil facilitate flushing and uniform heat distribution; as a result, the composite had a R_a of 2.52 μm compared to 2.86 μm when machined with conventional EDM oil. Surface topography showed the specimen machined with hydrocarbon dielectric medium proffers black spots, which were eliminated in castor dielectric medium. Best parametric combination was selected by the Relative Index Method optimization technique.

1. Introduction

Due to its low density and superior mechanical qualities, demand for magnesium alloy in the aerospace and automobile industries upsurged as it is used for the manufacturing of electronic frame, spacecraft machinery production, and ground transports. The addition of reinforcing particles to the magnesium alloy improves its strength-to-weight ratio and its ability to withstand high temperatures [1]. Despite the fact that magnesium is a rather soft material, machining magnesium-based metal matrix composites was tough [2]. When machined with conventional machining techniques, the removal of reinforced particles causes deeper craters on the machined surface, lowering surface quality, and increases tool wear rate [3]. Electric Discharge Machining (EDM) is an unconventional machining technique that can machine composites with high precision and accuracy [4]. Current, pulse-on time, pulse-off time, gap distance, and voltage are the distinct process parameters, which impacts the EDM performance [5]. When the current was supplied, dielectric breakdowns occurred after the breakdown voltage was achieved, resulting in the formation of a spark and the material removed by melting and evaporation [6]. During machining, a temperature of 10000°C was attained between the spark gaps.

Hydrocarbon oil and kerosene are the most commonly utilized EDM dielectric fluid. When exposed to a very high temperature, dielectric fluid decomposes and contaminates the atmosphere around the machine [7]. The deposition of carbon on the work surface hinders the discharge energy; hence, machining efficiency reduces [8]. Polanga dielectric fluid has a larger discharge energy density and a higher voltage breakdown band. It also has a higher oxygen concentration, which causes intense oxidation [9]. Water-based

dielectric fluid facilitates the electro chemical reaction, which reduces white layer thickness and enhances surface quality [10]. Deionized water deposited a layer of TiO_2 on the machined surface, lowered the discharge energy [11]. Addition of urea to the dielectric fluid enhanced the mechanical characteristics of machined titanium alloy surfaces [12]. Canola and sunflower-based dielectric fluid proffers higher MRR and lower TWR owing to its higher density [13]. Materials machined with gas media dielectric fluid exhibit very poor surface quality [14]. Materials machined under nitrogen gas medium improve the surface quality by eliminating the cracks on the surface [15].

Incorporation of foreign particles in the dielectric fluid improves the machining performance [16]. The powders Al_2O_3, Gr, SiC, and Al are added in the dielectric fluid to enhance machining efficiency [17]. The material removal mechanism in the EDM process affected by the type and concentration of the powders dispersed in the dielectric medium. Powder mixed electric discharge medium (PMEDM) produced craters on the machined surface with a smaller diameter and depth than traditional EDM [18]. The graphite particles contained in dielectric fluid shatter a single spark into several little sparks that crater on the machined surface, resulting in reduced surface roughness. On the other hand, a larger graphite content lowers the MRR and raises the kerf breadth [19]. The addition of alumina powder to dielectric fluid increases the distance between the electrodes due to the bridging effect, which reduces the Ra [20]. Because of its improved electrical and thermal conductivity, Cu powder mixed deionized water dielectric improves MRR by uniformly distributing electrical and thermal energy in the machining zone [21].

EDM, an unconventional machining method, employs an electric spark to remove material from work pieces that are conductive in nature and have no direct contact with each other. Suitable combination of tool and workpiece enhances the machining performances [22]. Cu, Br, Gr, W–Cu, W, Al, and Zn are the various materials used as the EDM electrode [23]. The thermophysical property of the electrode materials has a significant impact on EDM performance [24]. The influence of several tool materials (graphite, tungsten-copper, and brass) and process parameters on the machining properties of die steels (H11, HCHCr, and AISI 1045) was studied by Batish et al. [25]. After machining, they looked at material migration, surface morphological changes, grain size, and microstrain [26]. They discovered that tungsten-copper electrodes had higher MRR and overcut than graphite and brass electrodes, and that brass electrodes have lower TWR than graphite and tungsten-copper electrodes. Hascalk and Caydas [27] used graphite, electrolyte copper, and aluminium electrodes to perform EDM on titanium alloy (Ti–6Al–4V). They advocated using graphite electrodes to achieve better MRR, lower TWR, and reduced surface fracture density. The graphite tool produced the best results in terms of white layer thickness, surface fracture density, and SR. As a result, it is not advised for use under the stated operating conditions. With regard to the surface integrity, the brass tool performed best, followed by the copper tool [28].

The Technique for Order of Preference by Similarity to Ideal Solution (TOPSIS), multi-objective optimization on the basis of ratio analysis (MOORA), and grey relational analysis (GRA) are the various optimization technique used by the researchers to find out the best alternative from the available resources [29–31]. TOPSIS determines the best solution based on the distance between the ideal solution and the nonideal solution, MOORA provides a foundation for comparing options, making it easier to pick the optimal option, and GRA does not seek to identify the best solution; instead, it gives techniques for choosing a feasible solution to real-world problems. The common steps followed in the optimization techniques were normalization, weighted normalization, comparison, calculation of assessment value, and ranking of alternatives [32]. Literature review revealed that lot of works has been carried out by the researchers by varying dielectric fluid, tool materials, and varying process parameters. Even though survey related to machining of AZ91/5B_4C/5Gr hybrid composites under castor oil (CO) dielectric medium was scarcely available. Incorporating Al_2O_3 powder in CO to enhance the machining performance was the novel approach. In this research work, EDM of AZ91 hybrid composites was performed under castor oil dielectric medium (CDM) by varying tool materials, Al_2O_3 concentration, polarity, current, pulse-on time, and gap distance. The results were compared with the hydrocarbon oil discharge medium (HCDM), and optimized using Relative Index Method (RIM) optimization technique. The surface topography was analysed with the aid of scanning electron microscope (SEM).

2. Experimental Work

AZ91 magnesium alloy procured from the perfect metal alloys, Bangalore, with the chemical composition portrayed in Table 1 was selected as the matrix material. AZ91 alloy was placed in the graphite crucible and heated to the temperature of 600°C in Argon-protected environment. B_4C and Gr of average particle size 2 μm, as procured from Bhukhanvala industries, Mumbai, were selected as reinforcements as portrayed in Table 2. The particles were heated to the temperature of 250°C to remove the moisture content in it. To increase the wettability of the matrix and reinforcements, 2 wt% of potassium titanium fluoride (K_2TiF_6) was added as flux. The mixture was stirred using the mechanical stirrer at the speed of 600 RPM for 5 minutes as depicted in Figure 1. The melt was bottom poured into preheated mould made of die steel. The manufactured composites were turned and faced to eliminate its surface defects. The casting process parameters are shown in Table 3. EDM experiments were performed on the composites by varying dielectric medium, tool materials, Al_2O_3 powder concentration, tool materials, polarity, current, pulse-on time, and gap distance. Dielectric fluids, castor oil (CO), and hydrocarbon oil (HCO) were purchased from Dev International and Lubrall Industries, respectively. The L36 Taguchi mixed orthogonal array was used to design experimental runs as shown in Table 4, and each run was repeated for three times. Taguchi array that allows a finite number of combinations of various features at

Table 1: Chemical composition of AZ91.

Al	Cu	Zn	Fe	Ni	Mn	Si	Mg
9.17	0.02	0.91	0.004	0.002	0.33	0.087	Remaining

Table 2: Material specification.

S.No	Material	Form	Size
1	AZ91 magnesium alloy	Plate	100 mm × 10 mm x 6 mm (l mm x b mm x t mm)
2	Boron carbide (B_4C)	Powder	2 μm
3	Graphite (gr)	Powder	2 μm
4	Potassium titanium fluoride (K_2TiF_6)	Powder	0.5 μm

Figure 1: Pictorial view of magnesium stir casting setup.

various phases and to make sure that each level of each element is taken into account equally, owing to its balanced approach, and the fractionality of the design and the components may be assessed independently of one another. The specimens were machined for 10 minutes, and the average value was documented as MRR, TWR, and Ra. The MRR and TWR were calculated using equations (1) and (2) [33], which was the ratio of heft difference afore and after machining to the product of machined time and density. The heft of the work piece and tool was determined using electronic weighing equipment with a 0.0001 g precision. The Ra was measured using the SJ210 surface roughness tester, which has a 5% accuracy. Surface topography was analysed using the SEM, and best parametric combination was identified using RIM optimization technique.

$$\text{MRR} = \frac{W_b - W_a}{\rho * t}, \quad (1)$$

$$\text{TWR} = \frac{T_b - T_a}{\rho * t}, \quad (2)$$

where W_b and W_a are heft of the specimen afore and after machining (mg), T_b and T_a are heft of the tool afore and after machining (mg), ρ represents density of the material (kg/m^3), and t represents machined time (Min). The unit of MRR and TWR was mm^3/min.

Table 3: Stir casting process parameters.

Parameters	Values
Magnesium melting temperature	600°C
Preheating temperature of B_4C	250°C
Preheating temperature of gr	400°C
Stirring speed	600 rpm
Stirring time	5 Minutes
Stirrer	4 arm mechanical stirrer
Preheating temperature of mould	250°C

3. Results and Discussion

3.1. Influence of Various Process Parameters on the MRR of AZ91 Hybrid Composites. When the voltage was applied, a spark was generated in the gap distance, and the work piece was machined by melting and vaporization. Flushing and cooling of the work piece were the primary function of the dielectric fluid. Furthermore, it maintains the gap distance, ensuring steady and regulated ionization. The generated spark was held inside the gap distance for material removal, referred to as pulse-on time, and the charge was turned off to facilitate flushing, alluded to as pulse-off time. The mean MRR of composites machined in CDM was 0.230 mm^3/min, which was 5.5% higher than the MRR of samples machined in HCDM as shown in Figure 2. It was attributed to the following facts: (i) owing to the high thermal conductivity of CO, it facilitates the dissipation of generated heat to the work piece [34]; (ii) because of the lower dielectric strength of CO, machining cycle occurred at faster rate [35]; (iii) owing to high kinematic viscosity of CO, it transfers the generated heat more efficiently than the EDM oil [36]. Table 5 shows the properties of the dielectric fluid.

When the Al_2O_3 particles were incorporated in the dielectric fluid, it improves the MRR of composites in both the dielectric media. When a voltage applied to these particles, they become electrified and travel in a zigzag pattern and trigger the bridging effect, which increases MRR [37]. At the concentration of 6 g/l, specimen machined under powder mixed hydrocarbon oil discharge medium (PMHCDM) exhibits the MRR of 0.271 mm^3/min, which was 9.8% higher than the powder mixed castor oil discharge medium (PMCDM) machined samples. The addition of Al_2O_3 particles to the lower dielectric strength CO induces the

Table 4: EDM process parameters and its levels.

Factors	Unit	Levels		
		1	2	3
Current	(A)	8	16	24
Gap distance	(mm)	3	4	5
Pulse-on	(μs)	3	6	9
Al_2O_3 powder concentration	(g/l)	2	4	6
Tool material		Brass (Br)	Copper (Cu)	Graphite (Gr)
Dielectric fluid		Hydrocarbon oil (HCO)	Castor oil (CO)	—
Polarity		Positive	Negative	—
Machined time	(min)		10	

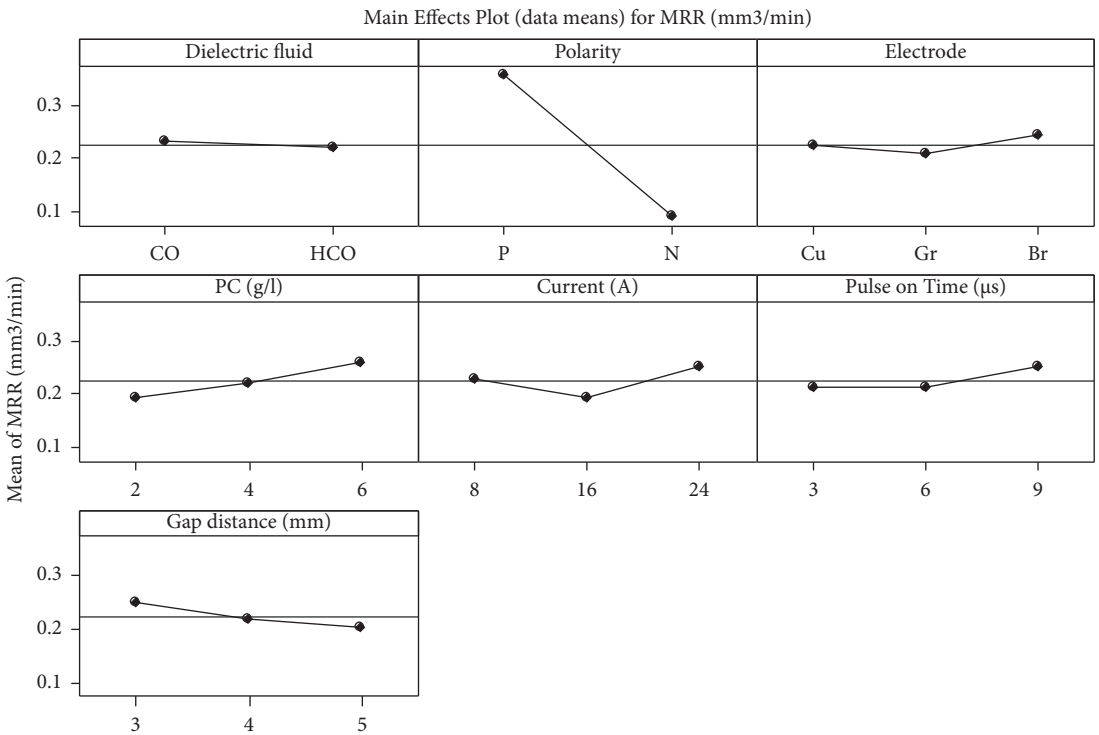

Figure 2: Impact of various process parameters on the MRR of AZ91 hybrid composites.

Table 5: Properties of di-electric fluid.

S.No	Properties	EDM oil	Castor oil	Benefits of utilizing castor oil as a dielectric
1	Colour	Colourless	Light yellow colour	Work piece was not visible; hence, it is a nonfavourable condition
2	Flash point	113□C	147□C	Higher flash point increases labour protection
3	Density	810 kg/m^3	987 kg/m^3	High density improves flushing
4	Dielectric strength	45 kVA	23 kVA	Higher dielectric strength increases machining efficiency, its nonbeneficiary
5	Kinematic viscosity at 40 ˚C	2.37 mm^2/s	16.64 mm^2/s	High viscosity increases heat transfer but reduces flushing; hence, it is a nonbeneficiary
6	Carbon content	90%	12–18%	High carbon content leaves black spots on machined surface
7	Thermal conductivity	0.124 W/ mk	4.727 W/mk	High thermal conductivity enhances heat dissipation
8	Specific heat	2.06 kJ/kg K	0.089 kJ/kg K	Castor oil has a lower specific heat than EDM oil, which is a beneficiary

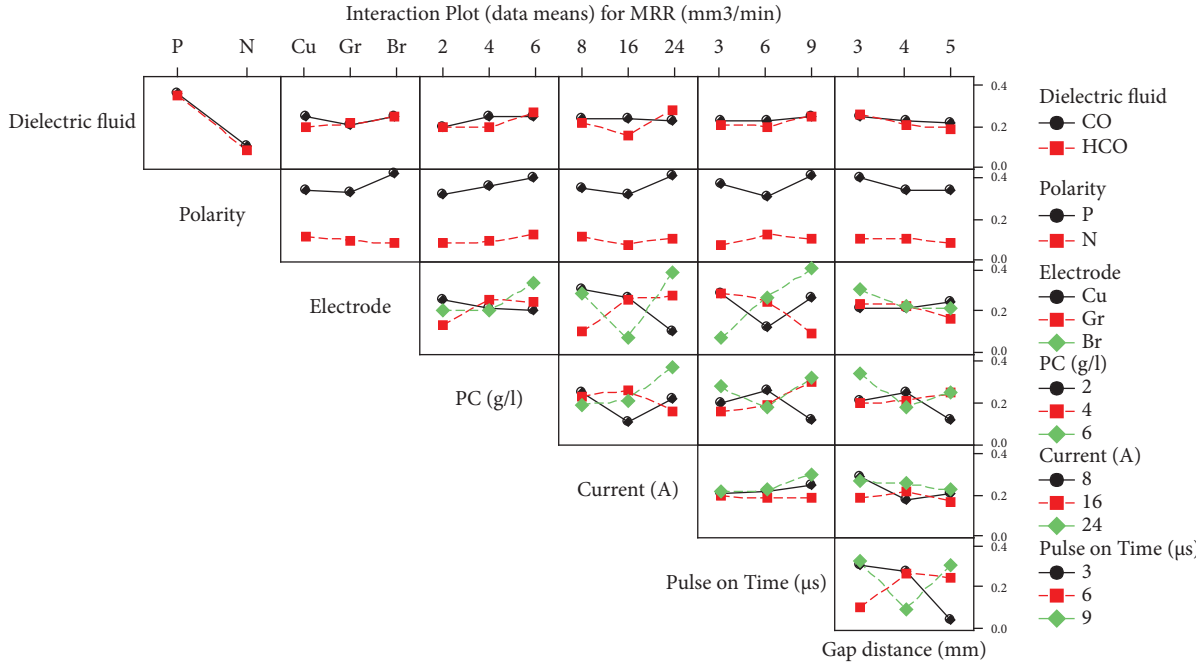

Figure 3: Interaction effect of distinct process parameters on MRR of AZ91 hybrid composites.

occurrence of cycles at a significantly faster rate, which hinders the machining performance. In case of PMHCDM, transformation from modest to extreme machining rate was observed when there was increase in Al_2O_3 concentration from 4 g/l to 6 g/l. At higher concentration, owing to the bridging effect, it generates the heat of very high intensity; hence, MRR increases.

Of the three electrodes, specimen machined under HCDM with Br electrode proffers high MRR followed by the Gr and Cu electrode, respectively. It was attributed to Br's low thermal conductivity of 150 W/mk, which meant most of the generated heat was transferred to the work piece, resulting in a high MRR [38]. Therefore MRR reduces, as Gr (262 W/mk) and Cu (387 W/mk) were used as the electrode material. In case of CDM, a maximum MRR was recorded when Cu was employed as the electrode followed by the Br and Gr electrode. Because of the high thermal conductivity of Cu electrode and lower dielectric strength of the fluid, high spark recurrence rate can be sustained in a tiny machining area, which enhances the MRR [39].

Interestingly, when Cu was used as the electrode, the MRR reduces with increase in the powder concentration of Al_2O_3 as shown in Figure 3. Because the Cu electrode absorbed the majority of the generated heat, heat transfer to the specimens was limited, and the MRR decreased. When other two electrodes were employed, the MRR increases with raise in powder concentration. With regard to current, when EDM was utilized as the dielectric fluid, MRR decreases until a saddle point of 16A increases. In case of CO, the MRR slightly reduces with increase in current. The results revealed that the current has very minimum impact on MRR under CDM.

The MRR increases with rising Ton and progresses from mild to severe when Ton is increased from 6 μs to 9 μs, regardless of dielectric fluid. At high Ton, the generated heat hold inside the spark gap for extended period of time; hence, the MRR increases. When the gap distance was tuned at 3 mm, the MRR of 0.251 mm^3/min was observed and it was reduced to 0.203 mm^3/min for 5-mm gap distance. At lower gap distance, intensified discharge energy struck the work piece, and with increase in gap distance, intensification of discharge reduces; hence, the MRR reduces [40]. With the incorporation of Al_2O_3 particles, the gap distance reduces owing to the bridging effect, which raises the MRR. Lower MRR was attained when electrodes were connected to the negative polarity, and similar results were observed by the various researchers. When electrodes were connected to the negative polarity, dielectric strength, viscosity, powder particle incorporation, and concentration, discharge intensity has no contribution towards the improvement of the MRR.

3.2. Influence of Various Process Parameters on the TWR of AZ91 Hybrid Composites. The objective of the EDM industry was to reduce the TWR without compromising the MRR. When materials machined under CDM, electrode exhibits higher TWR in comparison with HCDM machined condition as depicted in Figure 4. As discussed earlier owing to the lower dielectric strength of CO machining cycle occurred at faster rate, which removes material from the work piece as well as from tool material. Of three electrode materials selected for the investigation, Cu possess least TWR followed by the Br electrode owing to its high melting temperature [41]. When Gr electrode was employed, the larger proportion of generated heat was transferred to the electrode, hence wear rapidly. As a result, specimens machined with Gr electrode have lower MRR, as demonstrated by the

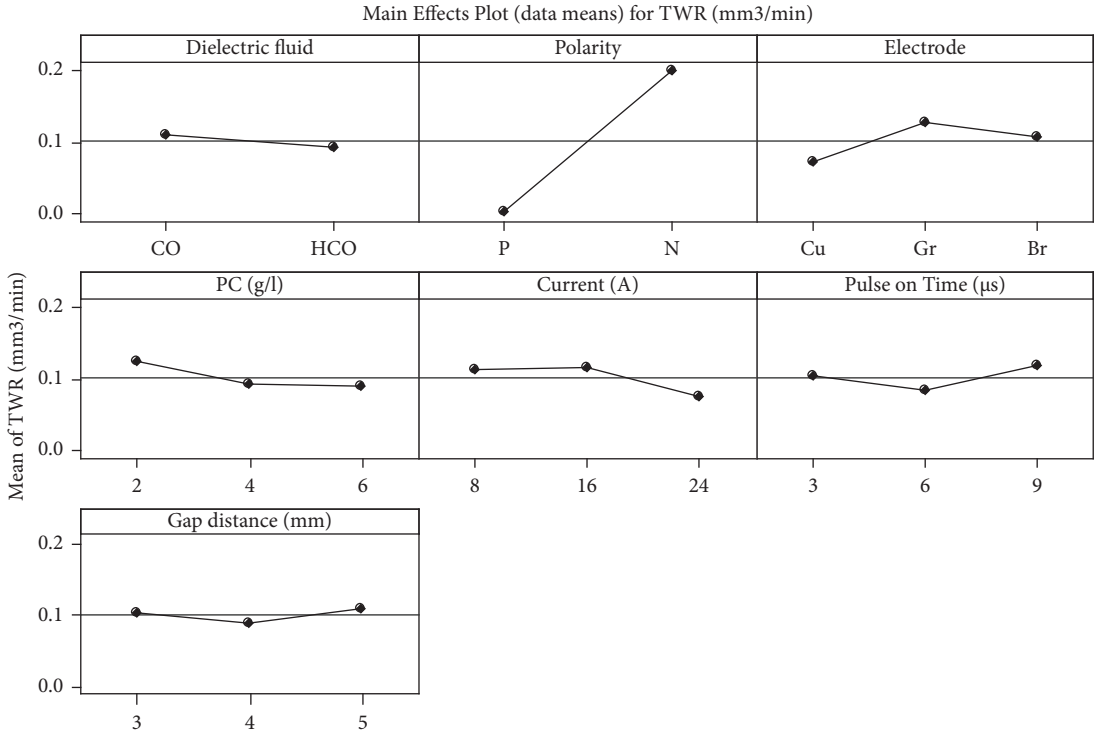

Figure 4: Impact of various process parameters on the TWR of AZ91 hybrid composites.

experimental data. The interaction plot reveals that Gr and Cu tools have lower TWR in HCDM, while Br has the lowest TWR in CDM.

TWR decreases as the concentration of Al_2O_3 particles increased pertaining to the objective. As discussed earlier, adding foreign particles triggers bridging effect, which reduces the gap distance between the tool and work piece [42]. In order to maintain the machining gap, spark distance increases, which reduces the discharge intensity on the tool material; hence, TWR reduces. In case of Cu electrode, TWR raises with increase in the powder concentration. Owing to the high thermal conductivity, it absorbs the major proportion of the generated heat, therefore eroded at the faster rate in comparison with other electrode [43]. Interestingly, when 6 g/l Al_2O_3 was incorporated, TWR in PMCDM was lower than PMHCDM as presented in Figure 5. It was due to the fact that the adding Al_2O_3 increases the dielectric strength, which reduces the frequency of spark occurred. Henceforth, for the same parametric condition, the MRR reduces as portrayed in the experimental results.

TWR decreases with raise in the parametric value of current in both the dielectric mediums. As the discharge current increased, more materials were melted and evaporated from the tool and the work surface, but owing to bridging effect spark gap increased, resulting in reduction in TWR. When machined at lower parametric value of 8 A current, TWR increases with raise in the concentration of Al_2O_3 particles. At such parametric setup, barge plasma channel was generated [44], and its intensity increased with raise in powder concentration resulting in increased TWR. With increase in Ton, TWR reduces until the saddle point of 6μs; thereafter, it starts to increase regardless of the dielectric medium. When tuned above the saddle point, plasma channel densification occurred results in higher TWR.

TWR decreases until the gap distance of 4 mm, when CO was utilized as the dielectric fluid, then rises. In the case of HCDM, a contrary trend was found, that is, that TWR increases until a gap distance of 4 mm decreases. The change in trend was linked to the kinematic viscosity of the dielectric fluid. A huge increase in TWR was noticed when connected to negative polarity, and several researchers reported comparable findings [45, 46]. The results confirmed that the major proportion of generated heat was transferred to the specimen connected to the positive terminal. As previously stated, when electrodes were connected to the negative polarity, dielectric strength, electrode material, and powder particles have no contribution to the reduction of TWR.

3.3. Influence of Various Process Parameters on the R_a of AZ91 Hybrid Composites. Component produced with superior surface quality increases the lifetime of the product, composites were machined with an intention of attaining mirror finish. Composites machined under CO dielectric medium exhibit least Ra in comparison with HCDM as depicted in Figure 6. It was attributed to the following facts: (i) because of the higher density of CO, it facilitated the flushing of machined debris, resulting in reduction of remelted layer deposition on the surface [47], and (ii) owing to its high specific heat, the generated heat was uniformly distributed over the machined surface, which improves the surface quality [48]. Specimens machined with Gr electrode exhibit average Ra value of 2.54 μm, and it was increased to 2.65 μm and 2.87 μm when machined with Br and Cu electrode,

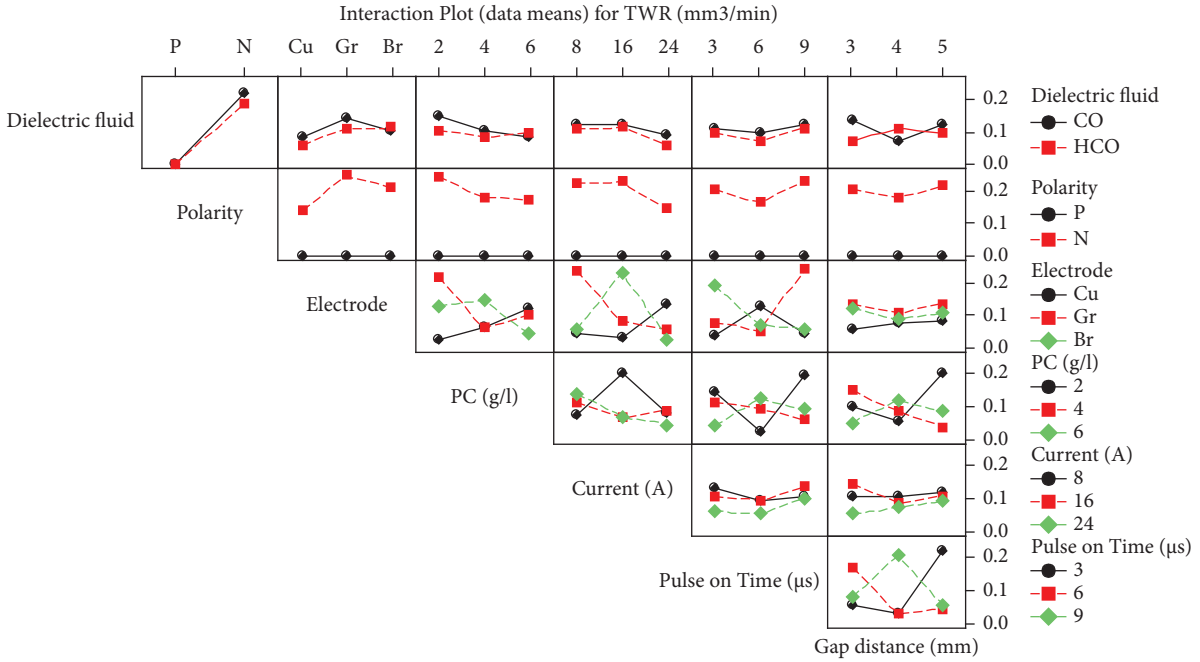

Figure 5: Interaction effect of distinct process parameters on TWR of AZ91 hybrid composites.

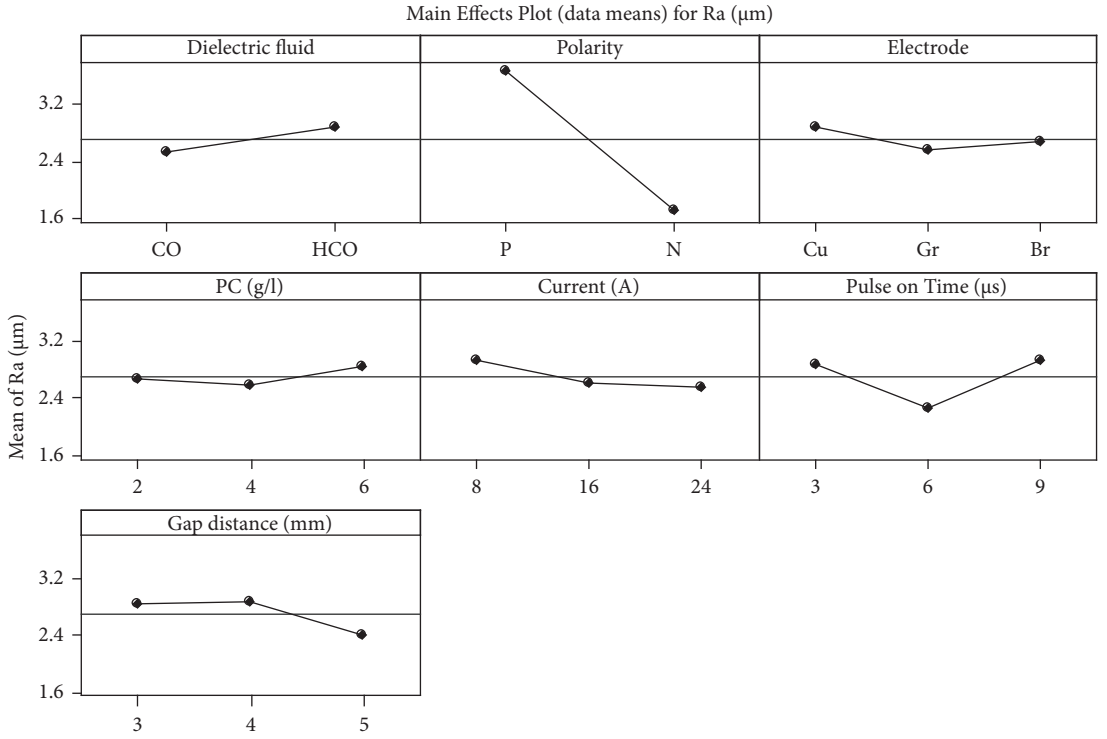

Figure 6: Impact of various process parameters on the Ra of AZ91 hybrid composites.

respectively. Because of the Cu electrode's superior thermal conductivity, very high intensity heat was generated, causing deeper craters and cracks to develop on the machined face, resulting in higher Ra value than a Br-machined specimen [49]. When machined with Gr electrode, as the majority of heat was passed to the tool material, the work piece was subjected to low spark, resulting in improved surface quality.

In PMCDM, Ra increases with raise in the Al_2O_3 powder concentration and reaches a maximum of 2.79 μm for the concentration of 6 g/l. With the incorporation of foreign particles, as machining continues the dielectric strength of the CO gets increased results in the improper flushing of machined debris; hence, Ra increases [50]. In case of PMHCDM, Ra reduces when 4 g/l of Al_2O_3 particles were

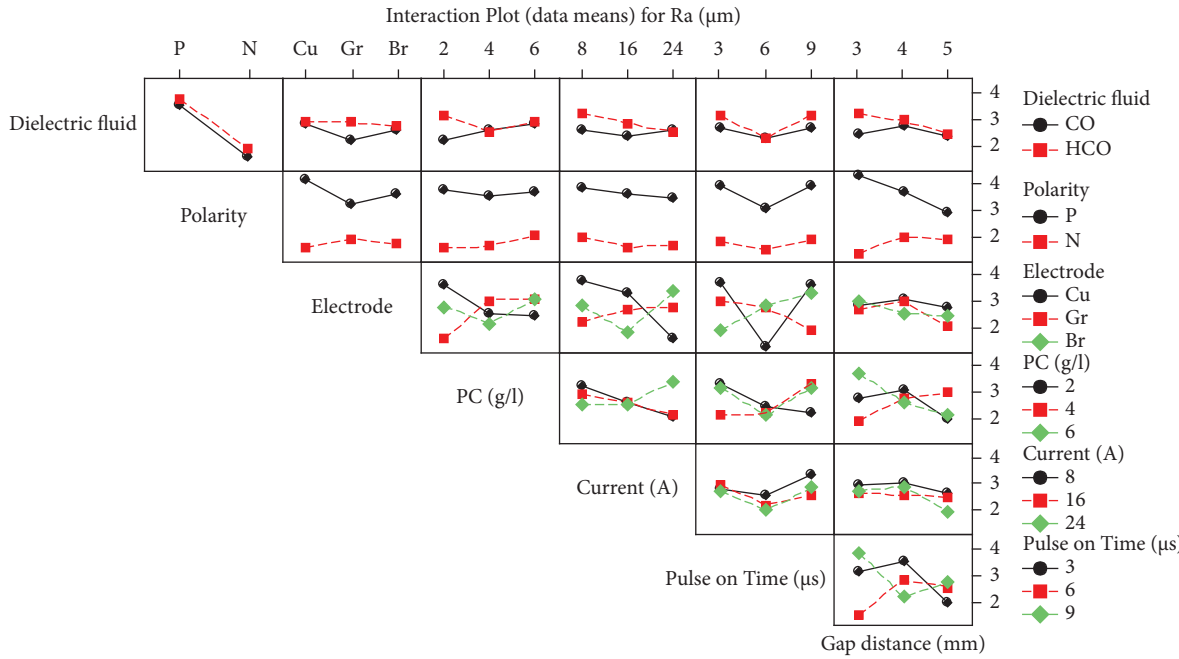

Figure 7: Interaction effect of distinct process parameters on Ra of AZ91 hybrid composites.

incorporated in the dielectric fluid. It was ascribed by the deed, and the bridging effect widened the spark gap, which facilitated the flushing of machined particles from the spark gap. Ra increases as the powder concentration was increased to 6 g/l due to densification of machined debris. The experimental results revealed that when machined with Gr electrode under 2 g/l PMCDM dielectric conditions, a mean $_{Ra}$ of 1.55 μm was obtained as shown in Figure 7. In PMHCDM, the discharge energy per pulse increases as the peak current increases, resulting in deeper and larger overlapping craters. The inclusion of particles widens the spark gap, reducing the intensity of the discharge struck on the work piece; hence, Ra reduces [51]. In the instance of PMCDM, increased current removes a significant volume of material, resulting in machined debris densification. This debris was not completely flushed away; hence, Ra increases because of the formation of solidification layer.

Ra reduces with increase in Ton until the saddle point of 6 μs increases. At higher Ton generated, heat held on for the extended period of time. Ascribable to that rather than vaporization melting of materials occurred, resulted in materialization of remelted layer, leads to the reduction of machined surface quality [52]. The mean Ra decreases significantly from 2.82 μm to 2.39 μm as the gap distance increases from 3 mm to 5 mm. The greater the gap distance, the more machining debris is flushed away, resulting in improved surface quality. Similar findings were reported by the various researchers [53, 54]. When electrodes were connected to the negative polarity, the surface quality of machined composites is 1.12 times better than the samples machined with the positive polarity condition. The least Ra value of 0.87 μm and 1.17 μm was obtained for PMHCDM and PMCDM, respectively, in both the cases, and specimens were connected to the negative polarity. The experimental results confirmed that it was able to attain least Ra when connected to the negative polarity regardless of the powder concentration, dielectric medium, and the discharge intensity.

3.4. Surface Topography. The specimens with the highest and lowest Ra in PMHCDM and PMCDM were chosen for microstructural examination. The composites machined with brass electrode (Ex no—21) under 6 g/l PMCDM have a high MRR of 0.421 mm^3/min and a Ra of 3.74 μm. At the magnification of 100x, surface texture displays globules, which were formed owing to the inadequate flushing of machined debris as shown in Figure 8(a). Because the specimen was machined with a greater current of 24 A, the micrograph showed deeper pits, craters, and tiny cracks. It was evident when the materials machined with a larger parametric value of current degraded the machined surface quality. The texture also had pock marks and micropores caused by the release of entrapped gas. At the magnification of 1000x, resolidified materials were clearly visible on the machined surface as shown in Figure 8(b). The surface was highly uneven which exploited that the generated heat was not uniformly distributed over machined area. At the higher magnification of 5000x, pits were clearly visible and the size ranges from 10 μm–15 μm, and that apart, it also showed globules and craters as shown in Figure 8(c).

The specimen machined with the Cu electrode (Ex no. 35) under 2 g/l PMCDM has a least Ra of 1.08 μm. But at this parametric setting, attained MRR was lower than the TWR, which greatly reduces the productivity of the EDM industry. At 100x, surface morphology showed cracks, craters, and pits as shown in Figure 9(a). The size of the cracks and craters was substantially decreased, and hence, the surface

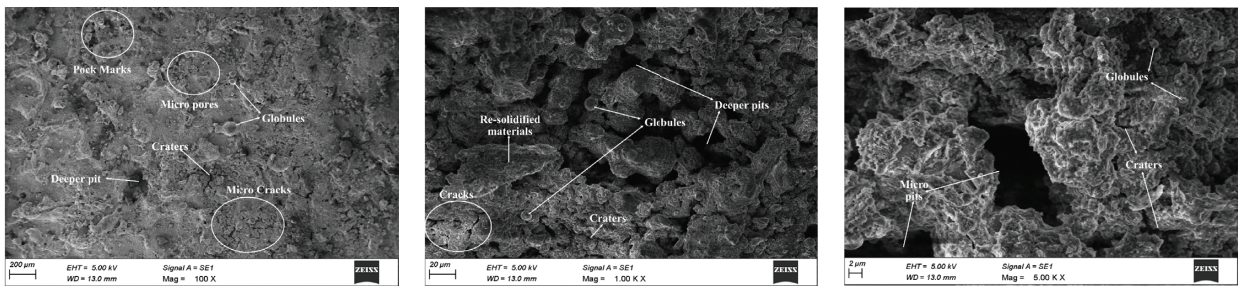

(a) (b) (c)

Figure 8: SEM of AZ91 hybrid composite machined in PMCDM using brass electrode. (a) At 100x. (b) At 1000x. (c) At 5000x.

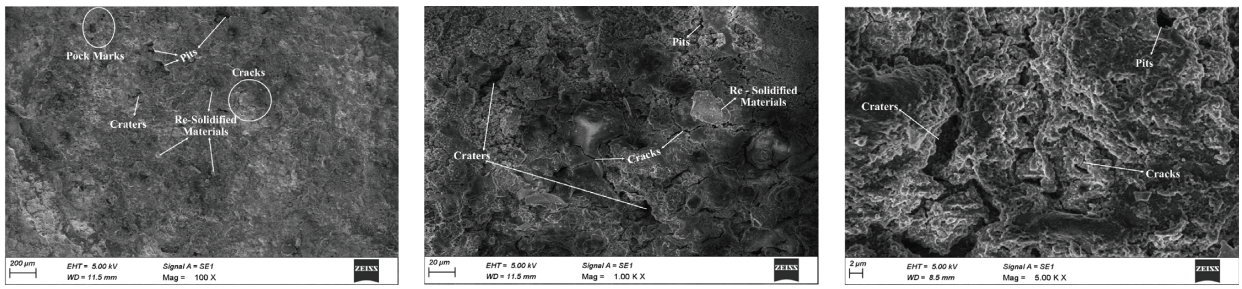

(a) (b) (c)

Figure 9: SEM of AZ91 hybrid composite machined in PMCDM using copper electrode. (a) At 100x. (b) At 1000x. (c) At 5000x.

quality increased. Pockmarks and tiny pits were the other features observed on the surface. At 1000x, resolidified materials were observed on the surface along with the smaller number of tiny pits as portrayed in Figure 9(b). The pits range in size from 2 μm to 6 μm, which is three times smaller than the pits formed at 6 g/l PMCDM. At 5000x, the texture resembles vitiligo skin, with a lot of white spots that were characterized as resolidified materials as depicted in Figure 9(c).

The sample machined using the Br electrode under PMHCDM (Ex no—6) exhibits MRR of 0.547 mm^3/min and a Ra of 5.42 μm. At 100x, the texture revealed a huge number of black dots on the surface, indicating that the carbon content on the surface was deposited HCDM as shown in Figure 10(a). When exposed to high temperatures, dielectric fluid decomposes and deposits carbon on the surface, hindering machining ability. A huge number of micropores and globules were also portrayed on the machined surface. At 1000x, deeper pits, globules of diameter ranges 5-6 μm, craters, and resolidified materials were observed as depicted in Figure 10(b). The deeper pits and high globule diameter portrayed sparks of greater intensity were produced, which effects the surface quality of the composites. At 5000x, crater valley length of about 50 μm was observed along with crack and pits as depicted in Figure 10(c), which impacts the quality of the surface.

When machined with Gr electrode at the powder concentration of 4 g/l (Ex no—11), composites exhibit Ra value of 2.21 μm, but the TWR was 5 times higher than the MRR. The texture showed micropits, resolidified layer, and lot of black spots on the surface as displayed in Figure 11(a). The presence of black spots indicates that hydrocarbon dielectric fluid decomposes at high temperatures regardless of the type of electrode used and the concentration of powder. At the magnification of 1000x texture displayed deeper pits, globules, craters, and resolidified materials as depicted in Figure 11(b). In comparison with other surfaces, the texture showed a deeper crater of 20 μm diameter. At further magnification of 5000x, approx. depth of the crater was estimated as 20 μm, which impacts the surface quality as shown in figure. The texture also showed redeposited materials, pits, and craters on the surface as shown in Figure 11(c). The tiny remelted layers are visible in all the specimens of SEM micrograph. The results revealed that when connect to the negative polarity, most of the machined specimens exhibit higher TWR in comparison with MRR. The comparison of the surface texture is shown in Table 6. When compared to other electrodes, the machined sample employing Gr electrode under PMHCDM connected to negative polarity displayed the most uniform and equal surface and produced the highest surface quality.

3.5. Relative Index Method. The best parametric combination was identified using the RIM optimization technique. As 36 experiments were conducted and machining performance accessed in terms of MRR, TWR, and Ra, a decisive matrix (X_{ij}) of 36×3 was formed as shown in Table 7 and its standard deviation with error bars is shown in Figure 12. The initial step was to compute range (R_{ij}) and set the ideal range (I_{ij}) as depicted in equations (3) and 4 [55].

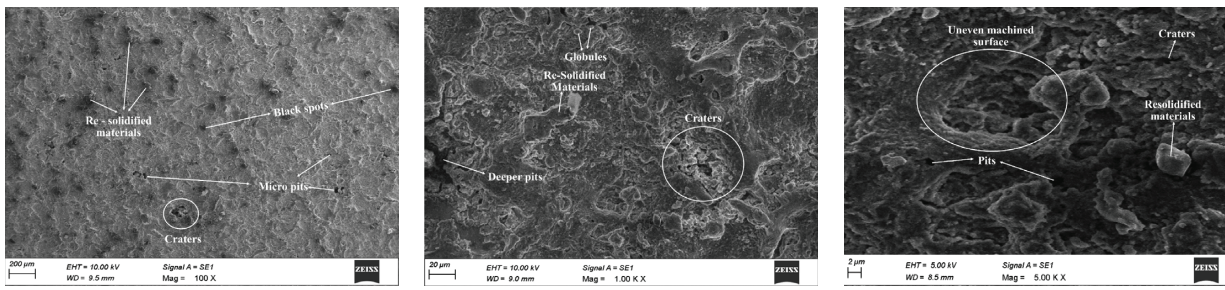

(a) (b) (c)

Figure 10: SEM of AZ91 hybrid composite machined in PMHCDM using brass electrode (a) At 100x. (b) At 1000x. (c) At 5000x.

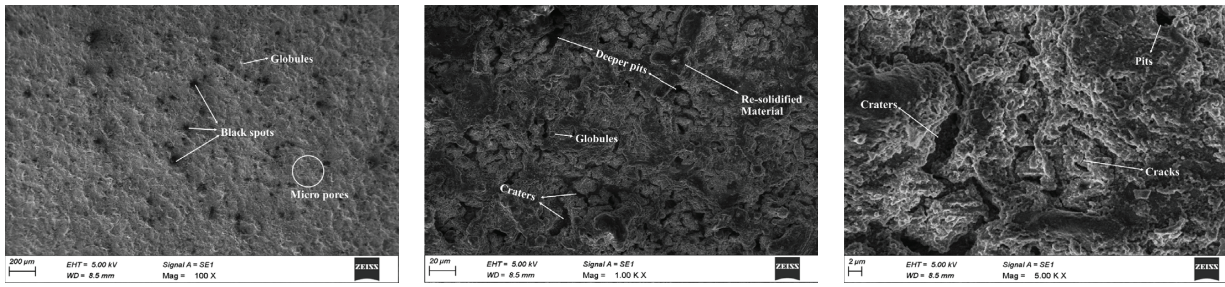

(a) (b) (c)

Figure 11: SEM of AZ91 hybrid composite machined in PMHCDM using graphite electrode (a) At 100x. (b) At 1000x. (c) At 5000x.

Table 6: Comparison of the surface texture.

Ex. No	Dielectric medium	Microstructure features		
		100x	1000x	5000x
21	PMCDM	Globules, deeper pits, craters, and tiny cracks	Resolidified materials	Pits of size 10 μm–15 μm
35	PMCDM	Tiny cracks, craters, and pits	Resolidified materials	Pits of size 2 μm–6 μm
06	PMHCDM	Black dots	Deeper pits, globules of diameter ranges 5–6 μm, craters, and resolidified materials	Crater valley of length about 50 μm
11	PMHCDM	Micropits, resolidified layer, and large number of black spots	Deeper crater of 20 μm diameter	Redeposited materials, pits, and craters

The ideal range was the value; if the estimated response falls within this limit, it is considered ideal. For example, in this problem, the maximum and minimum MRR were 0.547 mm^3/min and 0.032 mm^3/min, respectively, which was fixed as the range. If it is believed that achieving MRR greater than 0.451 mm^3/min improves productivity, then the ideal range was set at 0.451 mm^3/min and 0.547 mm^3/min, respectively.

$$R_{ij} = \left(\text{Max}\left(X_{ij}\right), \text{Min}\left(X_{ij}\right)\right), \tag{3}$$

$$I_{ij} = \text{Ideal}\left(X_{ij}\right), \tag{4}$$

$$Y_{ij} = \left(\left(I_{11} - X_{ij}\right), \left(I_{12} - X_{ij}\right)\right). \tag{5}$$

For beneficiary,

$$Z_{ij} = \text{Max}\left(Y_{ij}\right). \tag{6}$$

For nonbeneficiary,

$$Z_{ij} = \text{Min}\left(Y_{ij}\right). \tag{7}$$

The next step was the normalization of the decisive matrix. Normalization was accomplished by the following steps. The difference between the i^{th} element of the X row to the upper and lower circuit of the ideal matrix was calculated as the matrix of (Y_{ij}) (36×2) as shown in equation (5) [56]. For beneficiary attributes, matrix Z_{ij} was the maximum of Y_{11} and Y_{12}, whereas for nonbeneficiary minimum value was taken as portrayed in equations (6) and 7 [57]. Finally, normalized decision matrix N_{ij} was calculated. Followed by weighted normalized decision matrix (M_{ij}), it was computed which is the product of normalized value and weight of each criterion as per [58]

Table 7: Results of the performed EDM experiments.

Dielectric fluid	Polarity	Electrode	PC (g/l)	Current (A)	Pulse-on time (μs)	Gap distance (mm)	MRR (mm3/min)	TWR (mm3/min)	Ra (μm)
HCO	P	Cu	2	8	3	3	0.451	0.0011	4.37
HCO	P	Gr	4	16	6	4	0.332	0.0016	3.38
HCO	P	Br	6	24	9	5	0.483	0.0013	2.26
HCO	P	Cu	2	8	3	4	0.261	0.0021	4.44
HCO	P	Gr	4	16	6	5	0.233	0.002	2.93
HCO	P	Br	6	24	9	3	0.547	0.0017	5.42
HCO	P	Cu	2	16	9	3	0.211	0.0018	4.94
HCO	P	Gr	4	24	3	4	0.387	0.002	3.57
HCO	P	Br	6	8	6	5	0.294	0.0022	3.07
HCO	N	Cu	2	24	6	3	0.099	0.101	0.87
HCO	N	Gr	4	8	9	4	0.041	0.2392	2.21
HCO	N	Br	6	16	3	5	0.032	0.1681	1.42
HCO	N	Cu	4	24	3	5	0.061	0.1435	1.88
HCO	N	Gr	6	8	6	3	0.132	0.2106	2.42
HCO	N	Br	2	16	9	4	0.087	0.2345	1.39
HCO	N	Cu	4	24	6	3	0.101	0.1149	1.12
HCO	N	Gr	6	8	9	4	0.141	0.1861	2.79
HCO	N	Br	2	16	3	5	0.032	0.2695	3.01
CO	P	Cu	4	8	9	5	0.309	0.0023	4.32
CO	P	Gr	6	16	3	3	0.366	0.002	3.39
CO	P	Br	2	24	6	4	0.421	0.0031	3.74
CO	P	Cu	4	16	9	5	0.387	0.0027	2.83
CO	P	Gr	6	24	3	3	0.339	0.0018	3.68
CO	P	Br	2	8	6	4	0.256	0.0021	2.97
CO	P	Cu	6	16	3	4	0.376	0.0024	4.28
CO	P	Gr	2	24	6	5	0.287	0.0029	2.27
CO	P	Br	4	8	9	3	0.499	0.002	4.1
CO	N	Cu	6	16	6	4	0.088	0.1188	1.17
CO	N	Gr	2	24	9	5	0.074	0.2314	1.49
CO	N	Br	4	8	3	3	0.093	0.2221	1.09
CO	N	Cu	6	24	9	4	0.132	0.186	2.36
CO	N	Gr	2	8	3	5	0.057	0.3109	1.37
CO	N	Br	4	16	6	3	0.09	0.2694	1.42
CO	N	Cu	6	8	6	5	0.19	0.181	1.89
CO	N	Gr	2	16	9	3	0.087	0.3206	1.08
CO	N	Br	4	24	3	4	0.1	0.1091	1.99

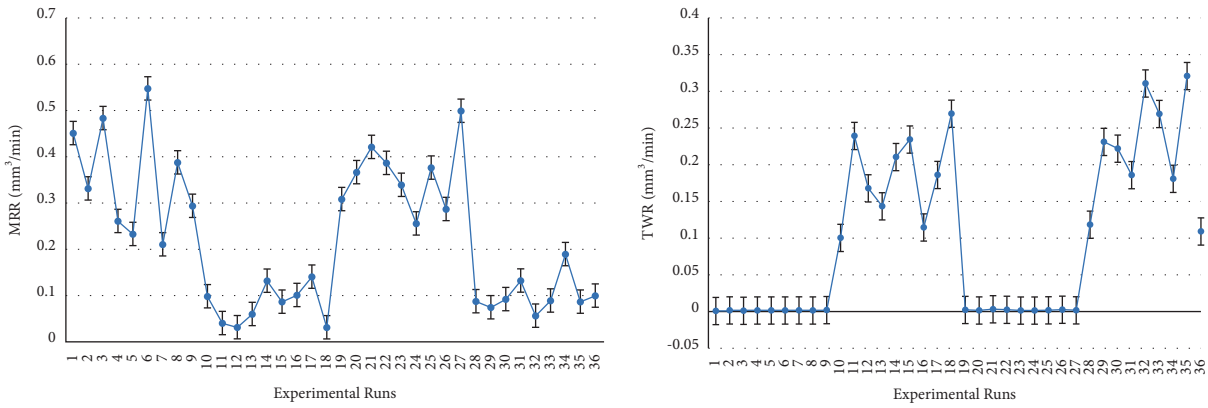

(a) (b)

Figure 12: Continued.

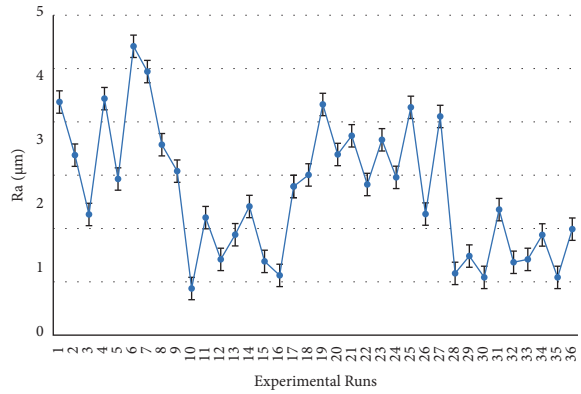

(c)

Figure 12: Standard deviation with error bars.

Table 8: Computation relative index value and ranking of alternatives.

S. No	Normalized decision matrix			Weighted normal decision matrix			W_{ij}	0.33	0.33	0.34
	MRR	TWR	Ra	MRR	TWR	Ra	Pre-assessment value		Index value	Rank
1	1	1	0.29745	0.33	0.33	0.10113	0.05706	0.228028	0.79986	13
2	0.71599	1	0.5779	0.23628	0.33	0.19649	0.02938	0.203334	0.87375	8
3	0.92363	0.99937	0.89518	0.3048	0.32979	0.30436	0.00191	0.294301	0.99357	1
4	0.54654	0.99875	0.27762	0.18036	0.32959	0.09439	0.08272	0.150066	0.64466	19
5	0.47971	0.99906	0.70538	0.15831	0.32969	0.23983	0.03951	0.191274	0.82879	11
6	1	1	0	0.33	0.33	0	0.1156	0.2178	0.65327	18
7	0.42721	0.99969	0.13598	0.14098	0.3299	0.04623	0.12203	0.130844	0.51743	25
8	0.84726	0.99718	0.52408	0.27959	0.32907	0.17819	0.02873	0.21821	0.88367	5
9	0.6253	0.99655	0.66572	0.20635	0.32886	0.22635	0.02821	0.201962	0.87745	6
10	0.1599	0.68862	1	0.05277	0.22724	0.34	0.08742	0.170024	0.66044	17
11	0.02148	0.25525	0.90935	0.00709	0.08423	0.30918	0.16562	0.102737	0.38283	32
12	1.1E-16	0.47821	0.86686	3.7E-17	0.15781	0.29473	0.1406	0.11177	0.44288	29
13	0.06921	0.55535	0.99717	0.02284	0.18326	0.33904	0.11588	0.149053	0.56261	23
14	0.23866	0.34494	0.84986	0.07876	0.11383	0.28895	0.11246	0.102653	0.47721	26
15	0.13126	0.26999	0.85836	0.04332	0.0891	0.29184	0.14254	0.094986	0.3999	31
16	0.16468	0.64503	0.92918	0.05434	0.21286	0.31592	0.09029	0.148068	0.62121	21
17	0.26014	0.42176	0.74504	0.08585	0.13918	0.25331	0.10354	0.090909	0.46753	27
18	1.1E-16	0.16024	0.68272	3.7E-17	0.05288	0.23212	0.19733	0.056678	0.22313	36
19	0.6611	0.99812	0.31161	0.21816	0.32938	0.10595	0.06729	0.167311	0.71318	15
20	0.79714	0.99906	0.57507	0.26305	0.32969	0.19552	0.02536	0.216123	0.895	4
21	0.9284	0.99561	0.47592	0.30637	0.32855	0.16181	0.03231	0.227993	0.87587	7
22	0.84726	0.99686	0.73371	0.27959	0.32897	0.24946	0.01074	0.248622	0.95859	2
23	0.7327	0.99969	0.49292	0.24179	0.3299	0.16759	0.03751	0.195381	0.83895	10
24	0.53461	0.99875	0.69405	0.17642	0.32959	0.23598	0.03441	0.195436	0.8503	9
25	0.821	0.9978	0.32295	0.27093	0.32928	0.1098	0.05648	0.193882	0.7744	14
26	0.60859	0.99624	0.89235	0.20084	0.32876	0.3034	0.01802	0.240468	0.93027	3
27	0.88544	0.99906	0.37394	0.2922	0.32969	0.12714	0.04674	0.210238	0.81812	12
28	0.13365	0.6328	0.91501	0.04411	0.20882	0.3111	0.09725	0.142339	0.59409	22
29	0.10024	0.27783	0.88669	0.03308	0.09168	0.30147	0.14644	0.100386	0.40671	30
30	0.14558	0.30699	0.93768	0.04804	0.10131	0.31881	0.13225	0.114211	0.46341	28
31	0.23866	0.42019	0.86686	0.07876	0.13866	0.29473	0.10178	0.112297	0.52456	24
32	0.05967	0.02854	0.85836	0.01969	0.00942	0.29184	0.20139	0.085648	0.29839	35
33	0.13842	0.15867	0.86686	0.04568	0.05236	0.29473	0.15997	0.091695	0.36435	33
34	0.37709	0.43587	1	0.12444	0.14384	0.34	0.07691	0.151775	0.66368	16
35	0.13126	−0.0019	0.94051	0.04332	−0.0006	0.31977	0.19191	0.104132	0.35175	34
36	0.16229	0.66134	0.97167	0.05356	0.21824	0.33037	0.089	0.159641	0.64204	20

Table 9: % Contribution of distinct process parameters on EDM machining performance.

S. No	Process parameters	Level 1	Level 2	Level 3	Maximum	Minimum	Influence	% Contribution
1	Dielectric fluid	11.31	11.96		11.96	11.31	0.65	5.97
2	Polarity	14.73	8.55		14.73	8.55	6.18	56.46
3	Electrode	8.03	7.63	7.60	8.03	7.60	0.43	3.93
4	PC (g/l)	8.03	7.63	7.60	8.03	7.60	0.43	3.93
5	Current (A)	7.46	7.22	8.59	8.59	7.22	1.37	12.51
6	Pulse-on time (μs)	7.47	8.62	7.19	8.62	7.19	1.43	13.06
7	Gap distance (mm)	7.46	7.91	7.90	7.91	7.46	0.45	4.13

$$M_{ij} = \left(W_{ij} * \left(1 - \left(\frac{Z_{ij}}{\mathrm{Max}\left(X_{ij}\right) - I_{12}} \right) \right) \right). \quad (8)$$

The next phase was the computation of pre-assessment values O_{ij} and P_{ij}. O_{ij} was the summation of the square of difference between the weighted normalized decision matrix and weight of each criterion as shown in equation (9). P_{ij} was the sum of the square of the weighted normalization decision matrix as shown in equation (10) [59]. Assessment value is the ratio of pre-assessment value (P_{ij}) to the summation of O_{ij} and P_{ij} as shown in equation (11) [60]. The parametric combination with highest assessment value as represented in Table 8 was chosen as the optimal as portrayed in equation (12) [61].

$$O_{ij} = \sum_{i=0}^{n} \left(M_{ij} - W_{ij} \right)^2, \quad (9)$$

$$P_{ij} = \sum_{i=0}^{n} \left(M_{ij} \right)^2, \quad (10)$$

$$Q_{ij} = \left(\frac{P_{ij}}{O_{ij} + P_{ij}} \right), \quad (11)$$

$$S_{ij} = \mathrm{Rank}\left(Q_{ij} \right). \quad (12)$$

The influential process parameter on the EDM machining performance was depicted in Table 9. From the results, it was confirmed that the polarity, which contributes to 56.46%, was the most influential process parameter followed by the Ton and current, which has contribution of 12.51% and 13.06%, respectively. The parameter, which has least impact on the machining parameters, was percentage concentration and electrode material with the percentage contribution of 3.93%.

4. Conclusion

(1) Specimens machined with CDM exhibit high MRR because of high thermal conductivity, high kinematic viscosity, and lower dielectric strength of the CO. Incorporation of Al_2O_3 particles in CDM and HCDM improves MRR because of the bridging effect. Employing Br as the tool materials enhances the MRR because of its lower thermal conductivity. When electrodes were connected to the negative polarity, composites proffer least MRR regardless of the parameter setting and type of dielectric fluid used.

(2) Br and Gr electrodes had lower TWR in CDM and HCDM, respectively. Because of its higher thermal conductivity, Cu electrode absorbs the majority of the generated heat as powder concentration increases, hence possess high TWR. When electrodes were connected to negative polarity, there was a significant rise in TWR.

(3) Ra of CDM-machined composites improves due to improved flushing and uniform heat dissipation. The work piece was subjected to minimal spark when machined with Gr electrode because the bulk of heat was transmitted to the tool material, resulting in enhanced surface quality. Due to the Cu electrode's greater thermal conductivity, very high-intensity heat was created, leading the machined face to develop deeper craters and fractures. Machined Ra of composites increased in PMCDM and decreased in PMHCDM as Al_2O_3 powder concentration increased.

(4) Pits, craters, pock marks, cracks, and resolidified materials were the distinct features observed on the surface topography. PMCDM machined specimen showed texture resembles the vitiligo skin, with a lot of white spots that were characterized as resolidified materials. The best parametric combination was identified using the RIM optimization technique.

Data Availability

All data are included in the manuscript.

Conflicts of Interest

The authors declare that they have no conflicts of interest.

References

[1] V. K. Bommala, M. G. Krishna, and C. T. Rao, "Magnesium matrix composites for biomedical applications: a review," *Journal of Magnesium and Alloys*, vol. 7, no. 1, pp. 72–79, 2019.

[2] T. Sathish, V. Mohanavel, K. Ansari et al., "Synthesis and characterization of mechanical properties and wire cut EDM process parameters analysis in AZ61 magnesium alloy+ B4C+ SiC," *Materials*, vol. 14, no. 13, p. 3689, 2021.

[3] T. Kellner, J. Kyncl, Z. Pitrmuc, L. Beranek, M. Kanak, and M. Kyncl, "Production process planning in additive

manufacturing and conventional machining technology manufacturing system," *Manufacturing technology*, vol. 19, no. 2, pp. 232–237, 2019.

[4] J. E. A. Qudeiri, A. H. I. Mourad, A. Ziout, M. H. Abidi, and A. Elkaseer, "Electric discharge machining of titanium and its alloys," *International Journal of Advanced Manufacturing Technology*, vol. 96, no. 1, pp. 1319–1339, 2018.

[5] J. E. Abu Qudeiri, A. Saleh, A. Ziout, A. H. I. Mourad, M. H. Abidi, and A. Elkaseer, "Advanced electric discharge machining of stainless steels: assessment of the state of the art, gaps and future prospect," *Materials*, vol. 12, no. 6, p. 907, 2019.

[6] H. Bisaria and P. Shandilya, "Experimental investigation on wire electric discharge machining (WEDM) of Nimonic C-263 superalloy," *Materials and Manufacturing Processes*, vol. 34, no. 1, pp. 83–92, 2019.

[7] B. Singaravel, K. C. Shekar, G. G. Reddy, and S. D. Prasad, "Experimental investigation of vegetable oil as dielectric fluid in Electric discharge machining of Ti-6Al-4V," *Ain Shams Engineering Journal*, vol. 11, no. 1, pp. 143–147, 2020.

[8] N. Ahmed, K. Ishfaq, K. Moiduddin, R. Ali, and N. Al-Shammary, "Machinability of titanium alloy through electric discharge machining," *Materials and Manufacturing Processes*, vol. 34, no. 1, pp. 93–102, 2019.

[9] B. P. Mishra and B. C. Routara, "Evaluation of technical feasibility and environmental impact of Calophyllum Inophyllum (Polanga) oil based bio-dielectric fluid for green EDM," *Measurement*, vol. 159, Article ID 107744, 2020.

[10] C. Li, X. Xu, Y. Li et al., "Effects of dielectric fluids on surface integrity for the recast layer in high speed EDM drilling of nickel alloy," *Journal of Alloys and Compounds*, vol. 783, pp. 95–102, 2019.

[11] G. Kibria, B. R. Sarkar, B. B. Pradhan, and B. Bhattacharyya, "Comparative study of different dielectrics for micro-EDM performance during microhole machining of Ti-6Al-4V alloy," *International Journal of Advanced Manufacturing Technology*, vol. 48, no. 5-8, pp. 557–570, 2010.

[12] K. V. Arun Pillai, P. Hariharan, and R. Krishna Murthy, "Micro ED milling of Ti-6Al-4V with SiC nano powder mixed dielectrics at different ranges of discharge energy," *Silicon*, vol. 13, no. 6, pp. 1827–1837, 2021.

[13] P. S. Ng, S. A. Kong, and S. H. Yeo, "Investigation of biodiesel dielectric in sustainable electrical discharge machining," *International Journal of Advanced Manufacturing Technology*, vol. 90, no. 9-12, pp. 2549–2556, 2017.

[14] Y. J. Lin, Y. C. Lin, A. C. Wang, Y. F. Chen, and H. M. Chow, "Machining characteristics of EDM using gas media," in *Advanced Materials Research*vol. 189, TransTech Publications Ltd, pp. 3123–3130, 2011.

[15] S. Fattahi and H. Baseri, "Analysis of dry electrical discharge machining in different dielectric mediums," *Proceedings of the Institution of Mechanical Engineers - Part E: Journal of Process Mechanical Engineering*, vol. 231, no. 3, pp. 497–512, 2017.

[16] P. S. Bains, R. Mahajan, S. S. Sidhu, and S. Kaur, "Experimental investigation of abrasive assisted hybrid EDM of Ti-6Al-4V," *Journal of Micromanufacturing*, vol. 2, no. 2, pp. 123–132, 2019.

[17] D. Devarasiddappa and M. Chandrasekaran, "Experimental investigation and optimization of sustainable performance measures during wire-cut EDM of Ti-6Al-4V alloy employing preference-based TLBO algorithm," *Materials and Manufacturing Processes*, vol. 35, no. 11, pp. 1204–1213, 2020.

[18] N. HuuPhan, T. Muthuramalingam, N. N. Vu, and N. Q. Tuan, "Influence of micro size titanium powder-mixed dielectric medium on surface quality measures in EDM process," *International Journal of Advanced Manufacturing Technology*, vol. 109, no. 3-4, pp. 797–807, 2020.

[19] P. Sivaprakasam, P. Hariharan, and S. Gowri, "Experimental investigations on nano powder mixed Micro-Wire EDM process of inconel-718 alloy," *Measurement*, vol. 147, Article ID 106844, 2019.

[20] A. Kumar, A. Mandal, A. R. Dixit, and D. K. Mandal, "Quantitative analysis of bubble size and electrodes gap at different dielectric conditions in powder mixed EDM process," *International Journal of Advanced Manufacturing Technology*, vol. 107, no. 7-8, pp. 3065–3075, 2020.

[21] A. P. Tiwary, B. B. Pradhan, and B. Bhattacharyya, "Influence of various metal powder mixed dielectric on micro-EDM characteristics of Ti-6Al-4V," *Materials and Manufacturing Processes*, vol. 34, no. 10, pp. 1103–1119, 2019.

[22] M. Bhaumik and K. Maity, "Effect of different tool materials during EDM performance of titanium grade 6 alloy," *Engineering Science and Technology, an International Journal*, vol. 21, no. 3, pp. 507–516, 2018.

[23] A. K. Sahu and S. S. Mahapatra, "Performance analysis of Cu-W-B4C composite tool during electrical discharge machining of titanium alloy," *Proceedings of the Institution of Mechanical Engineers - Part C: Journal of Mechanical Engineering Science*, vol. 235, no. 11, pp. 1992–2007, 2021.

[24] X. Wang, C. Li, H. Guo, S. Yi, L. Kong, and S. Ding, "Alternating energy electrical discharge machining of titanium alloy using a WC-pcd electrode," *Journal of Manufacturing Processes*, vol. 60, pp. 37–47, 2020.

[25] S. Jithin, S. S. Shetye, J. J. Rodrigues, K. S. Mhetre, S. A. Mastud, and S. S. Joshi, "Analysis of electrical discharge texturing using different electrode materials," *Advances in Materials and Processing Technologies*, vol. 4, no. 3, pp. 466–479, 2018.

[26] K. Shi, D. Zhang, and J. Ren, "Optimization of process parameters for surface roughness and microhardness in dry milling of magnesium alloy using Taguchi with grey relational analysis," *International Journal of Advanced Manufacturing Technology*, vol. 81, no. 1-4, pp. 645–651, 2015.

[27] N. Beri, S. Maheshwari, C. Sharma, and A. Kumar, "Technological advancement in electrical discharge machining with powder metallurgy processed electrodes: a review," *Materials and Manufacturing Processes*, vol. 25, no. 10, pp. 1186–1197, 2010.

[28] S. Dewangan, C. K. Biswas, and S. Gangopadhyay, "Influence of different tool electrode materials on EDMed surface integrity of AISI P20 tool steel," *Materials and Manufacturing Processes*, vol. 29, no. 11-12, pp. 1387–1394, 2014.

[29] V. R. Pathapalli, V. R. Basam, S. K. Gudimetta, and M. R. Koppula, "Optimization of machining parameters using WASPAS and MOORA," *World Journal of Engineering*, vol. 17, no. 2, pp. 237–246, 2019.

[30] N. Yuvaraj and M. Pradeep Kumar, "Multiresponse optimization of abrasive water jet cutting process parameters using TOPSIS approach," *Materials and Manufacturing Processes*, vol. 30, no. 7, pp. 882–889, 2015.

[31] N. Kaushik and S. Singhal, "Hybrid combination of Taguchi-GRA-PCA for optimization of wear behavior in AA6063/SiCp matrix composite," *Production & Manufacturing Research*, vol. 6, no. 1, pp. 171–189, 2018.

[32] M. Derick, C. Rani, M. Rajesh, M. E. Farrag, Y. Wang, and K. Busawon, "An improved optimization technique for estimation of solar photovoltaic parameters," *Solar Energy*, vol. 157, pp. 116–124, 2017.

[33] C. Somu, R. Ranjith, P. K. Giridharan, and M. Ramu, "A novel Cu-Gr composite electrode development for electric discharge machining of Inconel 718 alloy," *Surface Topography: Metrology and Properties*, vol. 9, no. 3, Article ID 035025, 2021.

[34] M. A. Razak, A. M. Abdul-Rani, and A. M. Nanimina, "Improving EDM efficiency with silicon carbide powder-mixed dielectric fluid," *International Journal of Machining and Machinability of Materials*, vol. 3, no. 1, pp. 40–43, 2015.

[35] F. L. Amorim, V. A. Dalcin, P. Soares, and L. A. Mendes, "Surface modification of tool steel by electrical discharge machining with molybdenum powder mixed in dielectric fluid," *International Journal of Advanced Manufacturing Technology*, vol. 91, no. 1-4, pp. 341–350, 2017.

[36] A. Abdudeen, J. E. Abu Qudeiri, A. Kareem, T. Ahammed, and A. Ziout, "Recent advances and perceptive insights into powder-mixed dielectric fluid of EDM," *Micromachines*, vol. 11, no. 8, p. 754, 2020.

[37] M. A. Razak, A. M. Abdul-Rani, A. A. Aliyu et al., "The potential of improving the Mg-alloy surface quality using powder mixed EDM," in *Progress in Engineering Technology*, Springer, Berlin, Germany, pp. 43–53, 2019.

[38] S. Rajamanickam and J. Prasanna, "Effect of conductive, semi-conductive and non-conductive powder-mixed media on micro electric discharge machining performance of Ti-6Al-4V," *International Journal of Electrochemical Science*, vol. 16, no. 3, Article ID 210317, 2021.

[39] V. D. Bui, V. Boehme, J. W. Mwangi, T. Berger, and A. Schubert, "Investigation of ultrasonic vibration assisted powder mixed electrical discharge machining for antibacterial coating on implant surfaces," *Procedia CIRP*, vol. 95, pp. 431–436, 2020.

[40] P. P. Mohanty, D. Mohapatra, A. Mohanty, and S. Nayak, "ANFIS-based modeling for prediction of surface roughness in powder mixed electric discharge machining," in *Computational Intelligence in Data Mining*, Springer, Berlin, Germany, pp. 151–159, 2020.

[41] A. Das, B. Tharra, V. S. R. Sammeta, and J. D. Barma, "Attribute of SiC powder additive mixed EDM on machining performance and surface integrity aspects of inconel 625," in *Recent Advances in Mechanical Engineering*, Springer, Berlin, Germany, pp. 869–879, 2021.

[42] A. T. Nguyen, X. H. Le, V. T. Nguyen et al., "Optimizing main process parameters when conducting powder-mixed electrical discharge machining of hardened 90CrSi," *Machines*, vol. 9, no. 12, p. 375, 2021.

[43] V. D. Bui, J. W. Mwangi, and A. Schubert, "Powder mixed electrical discharge machining for antibacterial coating on titanium implant surfaces," *Journal of Manufacturing Processes*, vol. 44, pp. 261–270, 2019.

[44] V. Tao Le, "The influence of additive powder on machinability and surface integrity of SKD61 steel by EDM process," *Materials and Manufacturing Processes*, vol. 36, no. 9, pp. 1084–1098, 2021.

[45] H. A. Sonawane and R. S. Pawade, "Effects of powder mixed dielectric on electro discharge machining (PMEDM) of HSS tool steel," *International Journal of Mechatronics and Manufacturing Systems*, vol. 5, no. 5/6, pp. 431–454, 2012.

[46] L. Upadhyay, M. L. Aggarwal, and P. M. Pandey, "Experimental investigations into rotary magnetic field and tool assisted electric discharge machining using magneto rheological fluid as dielectric," *International Journal of Mechatronics and Manufacturing Systems*, vol. 12, no. 1, pp. 1–19, 2019.

[47] S. Jain and V. Parashar, "Critical review on the impact of EDM process on biomedical materials," *Materials and Manufacturing Processes*, vol. 36, no. 15, pp. 1701–1724, 2021.

[48] S. Assarzadeh and M. Ghoreishi, "Modeling and optimizing powder mixed electrical discharge machining (PMEDM) process using neural networks," in *Proceedings of the 2nd Tehran International Congress on Manufacturing Engineering (TICME 2007) Iran University of Science and Technology*, Tehran, Iran, pp. 10–13, December 2007.

[49] S. T. Alam, A. N. Amin, M. I. Hossain, M. Huq, and S. H. Tamim, "Performance evaluation of graphite and Titanium Oxide powder mixed dielectric for electric disharge machining of Ti–6Al–4V," *SN Applied Sciences*, vol. 3, no. 4, pp. 1–12, 2021.

[50] V. D. Bui, J. W. Mwangi, A. K. Meinshausen, A. J. Mueller, J. Bertrand, and A. Schubert, "Antibacterial coating of Ti-6Al-4V surfaces using silver nano-powder mixed electrical discharge machining," *Surface and Coatings Technology*, vol. 383, Article ID 125254, 2020.

[51] L. L. Guo, Y. F. Cheng, X. Ren et al., "Simultaneous deposition of tannic acid and poly (ethylene glycol) to construct the antifouling polymeric coating on Titanium surface," *Colloids and Surfaces B: Biointerfaces*, vol. 200, Article ID 111592, 2021.

[52] E. M. Barkhudarov, I. A. Kossyi, A. M. Anpilov et al., "New nanostructured carbon coating inhibits bacterial growth, but does not influence on animal cells," *Nanomaterials*, vol. 10, no. 11, p. 2130, 2020.

[53] A. K. Meinshausen, M. Herbster, C. Zwahr et al., "Aspect ratio of nano/microstructures determines *Staphylococcus aureus* adhesion on PET and titanium surfaces," *Journal of Applied Microbiology*, vol. 131, no. 3, pp. 1498–1514, 2021.

[54] M. Al-Amin, A. M. Abdul-Rani, T. V. V. L. N. Rao et al., "Investigation of machining and modified surface features of 316L steel through novel hybrid of HA/CNT added-EDM process," *Materials Chemistry and Physics*, vol. 276, Article ID 125320, 2022.

[55] T. Hirschfeld, "Accuracy and optimization of the two prism technique for calculating the optical constants from ATR data," *Applied Spectroscopy*, vol. 24, no. 2, pp. 277–282, 1970.

[56] M. Prabhakar B S, R. Ranjith, and S. Venkatesan, "Characterization of electric discharge machining of titanium alloy utilizing MEIOT technique for orthopedic implants," *Materials Research Express*, vol. 8, no. 8, Article ID 086505, 2021.

[57] S. Chakraborty and S. Chakraborty, "A scoping review on the applications of MCDM techniques for parametric optimization of machining processes," *Archives of Computational Methods in Engineering*, vol. 29, no. 6, pp. 4165–4186, 2022.

[58] R. Ranjith and S. N. Vimalkumar, "Integrated MOORA-ELECTRE approach for solving multi-criteria decision problem," *World Journal of Engineering*, vol. 19, no. 4, pp. 510–521, 2021.

[59] S. Chamoli, "Preference selection index approach for optimization of V down perforated baffled roughened rectangular channel," *Energy*, vol. 93, pp. 1418–1425, 2015.

[60] R. Ranjith, C. Somu, G. Tharanitharan, M. Naveenkumar, and N. M, "Integrated Taguchi cum grey relational experimental analysis (GREAT) for optimization and machining characterization of cryogenic cooled AA6063 aluminium alloys," *Materials Today Proceedings*, vol. 18, pp. 3597–3605, 2019.

[61] L. H. J. Jeewantha, K. D. C. Emmanuel, H. M. C. M. Herath, M. M. Islam, L. Fang, and J. A. Epaarachchi, "Multi-attribute parametric optimisation of shape memory polymer properties for adaptive orthopaedic plasters," *Materialia*, vol. 21, Article ID 101325, 2022.